LIMNOLOGY
and
OCEANOGRAPHY: METHODS

Limnol. Oceanogr.: Methods 6, 2008, 162–171

In situ field measurements of aquatic animal-fluid interactions using a Self-Contained Underwater Velocimetry Apparatus (SCUVA)

Kakani Katija[1] *and John O. Dabiri* [1,2]*

[1]Bioengineering, California Institute of Technology, Pasadena, CA 91125, USA

[2]Graduate Aeronautical Laboratories, California Institute of Technology, Pasadena, CA 91125, USA

Abstract

We describe the development of a Self-Contained Underwater Velocimetry Apparatus (SCUVA) that enables a single SCUBA diver to make in situ digital particle image velocimetry (DPIV) measurements of animal-fluid interactions in real time. The device is demonstrated in a study of the dynamics of *Aurelia labiata* a jellyfish swimming in the coastal waters of Long Beach, California. We analyze the DPIV measurements by computing the kinetic energy in the flow field induced by an animal's swimming motions. As a proof-of-concept, we compare these results with an existing theoretical model and find that the results are consistent with one another. However, SCUVA provides details regarding the temporal evolution of the energetics during the swimming cycle, unlike the model. These results suggest the usefulness of SCUVA as a method to obtain quantitative field measurements of in situ animal-fluid interactions.

Introduction

The ability to directly measure physical interactions between aquatic animals and the surrounding fluid environment is necessary to provide empirical data for studies in fields as diverse as oceanography, ecology, biology, and fluid mechanics. However, field measurements introduce practical challenges such as environmental conditions, animal availability, and the need for field-compatible measurement techniques. To avoid these challenges, scientists typically use controlled laboratory environments to study animal-fluid interactions.

To increase measurement efficiency, researchers have devised methods to constrain animal movement in the laboratory. These techniques include placing animals in flumes (e.g., Drucker and Lauder 1999; Bartol et al. 2001; Tytell and Lauder 2004), tethering animals (e.g., Vogel 1966; Koehl and Strickler 1981; Daniel 1983; Yen et al. 2003), and free-swimming measurements with imposed flow conditions (e.g., Bundy and Paffenhofer 1996; Shadden et al. 2006). Traditional measurement techniques include dye visualizations (e.g., Didden 1979; Dabiri et al. 2005) and digital particle image velocimetry, or DPIV (e.g., Adrian 1991; Willert and Gharib 1991; Drucker and Lauder 1999; Dabiri and Gharib 2004). The computation of Lagrangian coherent structures (LCS) from the DPIV data has been recently shown to provide a robust method for quantifying the features of the flow field (e.g., Shadden et al. 2006; Peng et al. 2007).

Despite the prevalent use of laboratory measurements, it is reasonable to question whether one can extrapolate natural behavior (i.e., that which occurs in the field) from laboratory measurements. For example, it is known that the presence of tethers alters the flow fields of ciliated larvae (Emlet 1990) and affects the structure of LCS in the wake of a jellyfish (Katija and Dabiri 2006). Especially in unsteady swimming, boundary layer development and forces associated with overcoming the inertia of animal motion are altered when an animal is tethered. Catton et al. (2007) found differences in the strain rate fields between free-swimming and tethered copepods and noted the importance of studying free-swimming animals when making sensory ecology conclusions. Hence, at least in these cases and likely in others, a quantitative field measurement technique is needed to correctly characterize in situ behavior.

Quantitative field measurements using DPIV techniques have been achieved previously. A potential constraint in the field is the need for particles to track in the flow to implement DPIV. In coastal water, suspended particulate matter exhibits sizes on the order of 10 μm in diameter and concentrations between 0.002 and 10 per mm^3 (Agrawal and Pottsmith 1994). Additional studies using a submersible holocamera for particle

*Corresponding author e-mail: jodabiri@caltech.edu

Acknowledgments

The authors gratefully acknowledge field support provided by Jifeng Peng of Caltech and Mike Schaadt of the Cabrillo Marine Aquarium (San Pedro, CA). This work is supported by the NSF Ocean Sciences Division-Biological Oceanography (OCE-0623475 awarded to J.O.D.). K.K. is supported by a National Defense Science and Engineering Graduate Fellowship.

detection confirmed a sufficient presence of seeding particles to perform DPIV in ocean water (Katz et al. 1999). Submersible PIV systems have previously been designed to measure turbulence levels in the bottom ocean boundary layer, and to provide data on mean vertical velocity profiles and the time evolution of the mean velocity (Bertuccioli et al. 1999; Nimmo Smith et al. 2002). Free-falling platforms using a combination of measurements from planar laser-induced fluorescence and stereoscopic PIV have been used to observe and quantify microscale turbulence structures in the upper ocean (Steinbuck et al. 2004). In addition to these larger (apparatus weight on the order of 10^3 kg) and more expensive submersible DPIV devices, it has recently been proposed to use a small-scale submersible PIV system to characterize naturally occurring flows close to the shore (Clarke et al. 2007).

Existing field DPIV devices lack the functionality required to collect quantitative measurements of animal-fluid interactions. For example, these devices typically have physical connections (e.g., cables) between the submerged device and the surface, which limits the area that can be measured to a fixed radius around a surface connection point. Additionally, these devices are usually unable to actively track the movement of animals in real-time due to their large size and lack of agility and controllability. Hence, existing systems are typically kept in a stationary position, towed behind a vessel, or programmed to execute predefined sweeps for data collection. A self-contained, portable device that can actively track animals independent of any connection to the surface and that is able to provide quantitative measurements of the flow field surrounding an animal has not previously been developed to the best of the authors' knowledge. Here, we describe the development of a self-contained underwater velocimetry apparatus, or SCUVA, that achieves the goal of real-time, quantitative field measurements of aquatic animal-fluid interactions.

To demonstrate the developed method, we conducted a preliminary investigation of the potential role of animal-fluid energy interactions in ocean mixing, a topic of increasing study that has been limited by the need for in situ field data at the scale of individual animals. Mixing against ocean stratification requires an input of mechanical energy whose sources are traditionally attributed primarily to winds and tides (Munk and Wunsch 1998). Munk (1966) found that the production of energy by marine organisms was of the same order of magnitude as tidal energy dissipation but later deemed them as negligible contributors to abyssal mixing. Biological sources of ocean mixing continued to be overlooked until rates of kinetic energy production were calculated for representative species of schooling animals (Huntley and Zhou 2004). The biological rate of kinetic energy production of a broad range of schooling animals was found to be on the order of 10^{-5} W kg^{-1}, which was later confirmed by microscale shear measurements of a large concentration of krill (Kunze et al. 2006). These findings suggest that biosphere input to the ocean mixing energy budget may impact mixing at the same level as winds and tides, whose respective rates of kinetic energy production are of the same order (Dewar et al. 2006). However, the issue of biogenic mixing remains largely unresolved. To assess the potential of SCUVA to inform the ongoing debate regarding biogenic turbulent mixing, we study the dynamics of *Aurelia labiata* swimming in coastal regions near Long Beach, California. SCUVA measurements of *Aurelia labiata* are used to directly quantify the kinetic energy in the flow field induced by the swimming motions of individual medusae. The results are compared with the semi-empirical model predictions of Huntley and Zhou (2004).

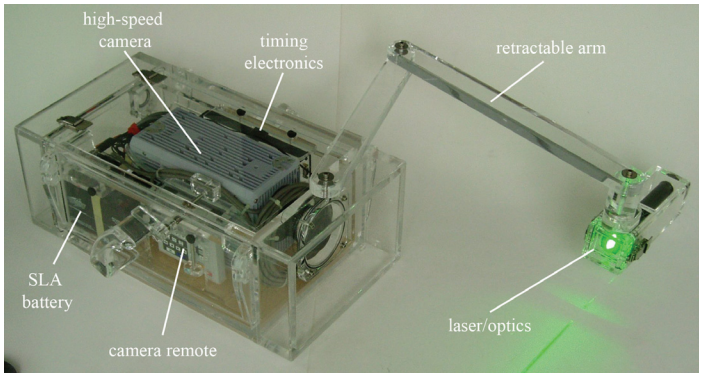

Fig. 1. SCUVA shown with laser arm extended and laser sheet activated

Materials and procedures

SCUVA components—Particle illumination by SCUVA is provided by a continuous 300 mW, 532 nm solid-state laser. The output laser beam is collimated into a planar sheet by a plano-concave cylindrical lens (effective focal length = –6 mm). Using the current optical configuration, the size of the illuminated region can be adjusted from 15 cm W × 15 cm H to as large as 60 cm W × 60 cm H. Still smaller or large viewing windows can be achieved by modifying the camera lens and laser position. The laser and optics are mounted in a waterproof housing at the end of a retractable arm that locks to ensure that the camera is focused on the plane of the laser sheet at all times (Fig. 1). The arm is collapsed while the SCUBA diver swims to the measurement site and subsequently extended to initiate measurements.

The flow field illuminated by the laser sheet is imaged by a high-speed camera (Photron APX-RS). The camera records images at a maximum resolution of 1024 × 1024 pixels at speeds up to 3000 frames s^{-1}. Higher speed recordings can be made at reduced spatial resolution. An electronic shutter enables exposure times as short as 1 μs, ensuring that particles can be imaged without any blurring. Recorded images are stored internally on an 8 GB hard drive. This capacity enables collection of 6144 full-resolution frames before the device must be surfaced to upload the stored measurement data. Control of the camera is achieved by a single START-STOP push-button control integrated into the right handle of the

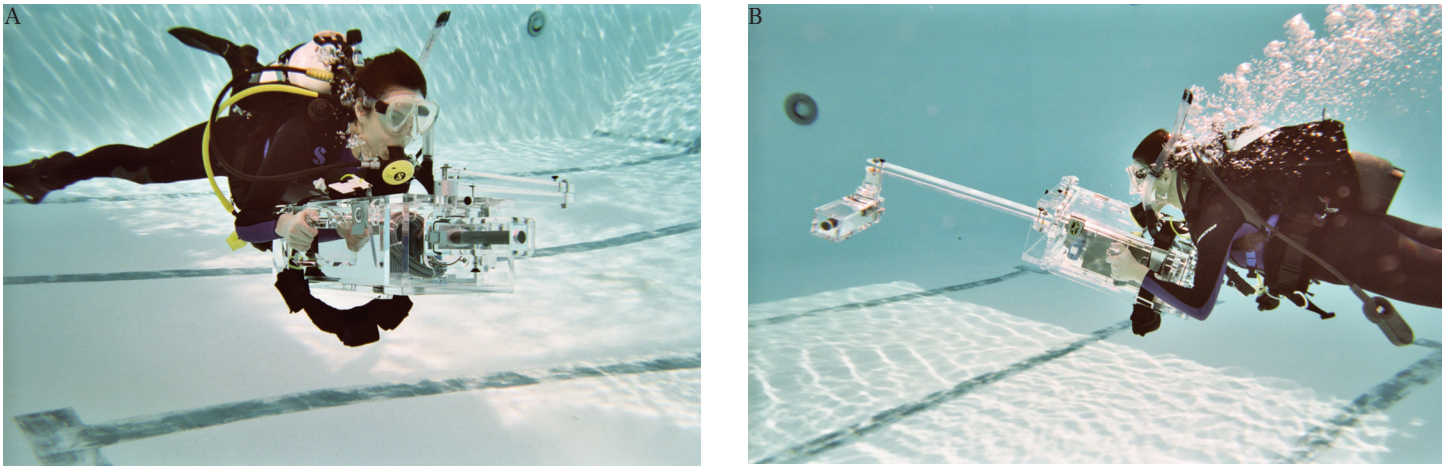

Fig. 2. Selected images from a swimming pool demonstration of SCUVA. (a) SCUVA with the laser arm in the stowed position; (b) SCUVA with the laser arm in the deployed position

main housing containing the camera. The camera is moisture-resistant and shock rated up to 100 g (980 m s^{-2}).

In order to measure a broad range of flow speeds in situ, timing electronics (Signal Forge 1000) have been integrated to ensure that particle displacements between adjacent frames can be optimally captured regardless of flow conditions. These electronics send a TTL trigger signal to the camera to initiate each image capture event. The duration between input trigger signals is made shorter for faster flow (i.e., so that particles do not travel too far in between frames) and longer for slower flow (i.e., so that a measurable change in particle position is achieved). The timing electronics are programmed on the boat/shore prior to initiating a dive.

The laser is powered by a rechargeable lithium-ion battery with a lifetime of 60 min starting from a full charge. This is sufficient for individual dive expeditions. In practice, several batteries are brought to the field so that recharging need not commence until after several dives. The camera and timing electronics are powered by a single 12 V, 10 A sealed lead acid rechargeable battery. This battery lasts marginally longer than the laser battery, and hence dive duration is limited by the laser power.

The housings (Sexton Photographics) for the camera and laser are both constructed from impact-resistant acrylic to ensure durability while maintaining relatively light weight and visual access to the SCUVA components. The retractable arm connecting the two housings is also constructed from acrylic. The rear of the camera housing contains several interfaces that enable interaction with the camera and battery without removing them from the housing. These include a gigabit ethernet link for data transfer to/from the camera, outlet for battery recharging, and on-off switches for the camera and timing electronics. In addition, a pair of one-way gas valves enable the air within the camera housing to be purged. This is useful for replacing ambient humid air with dry air, thereby reducing the effects of moisture condensation within the housing when it is submerged in cold water. Both the laser and camera housing can withstand water pressures at depths up to 40 m (4 atm gage pressure).

Figure 2 shows images from a demonstration of SCUVA in a swimming pool. For scale reference, the diver in this demonstration is 1.63 m tall.

Assessment

Field measurements—Specimens of juvenile *Aurelia labiata* (Chamisso and Eysenhardt, 1821), an oblate hydromedusa, were imaged using SCUVA off the coast of Long Beach, CA, USA (Lat 33.76°N Long 118.12°W) during the month of March 2007. Dives were conducted at night to ensure that the DPIV laser sheet was minimally affected by other light sources. All data were collected in shallow water (depths < 5 m). Relying on the presence of natural sedimentation to provide sufficient seeding density for DPIV, a single representative jellyfish swimming cycle (duration of 1 s) was analyzed in detail to provide proof-of-concept.

Data analysis—The images captured by SCUVA were processed with an in-house DPIV algorithm (Willert and Gharib 1991). The time between successive images (Δt) was 0.033 s. The DPIV interrogation window size was 32 × 32 pixels with a 50% overlap (16 × 16 pixel step size). The velocity and vorticity calculations introduce measurement uncertainties of 1% to 2% and 3% to 5%, respectively (Willert and Gharib 1991).

The velocity field captured by SCUVA (u_{scuva}) includes the actual motion of the fluid (u_{real}) as well as undesired motion of the camera (u_{cam}) that occurs due to movement of the diver during the measurements, i.e.,

$$u_{scuva} = u_{real} + u_{cam} . \quad (1)$$

Since the camera is rigid, it possesses six degrees of freedom in its motion: translation along three orthogonal axes in

space, and rotation about those three axes. Therefore, its velocity field u_{cam} is either spatially uniform (i.e., a constant) throughout the camera field of view, in the case of linear camera motion; or, a linear function of position within the camera field of view, in the case of rotational camera motion; or, a superposition of these two. This component u_{cam} of the measured velocity field must be subtracted from the SCUVA measurements to obtain the true fluid motion.

Before describing the motion correction that was implemented, it is worth noting that physically relevant derivatives of the measured velocity field (u_{scuva}) are either insensitive to the camera motion or else they explicitly indicate the effect of the camera motion. For example, in the case of linear camera motion, the measured vorticity field ω_{scuva} is equal to the real vorticity field ω_{real}, irrespective of the linear camera motion. This is because the vorticity field is determined by taking the mathematical curl of the velocity field, and the curl of the spatially uniform vector u_{cam} is identically zero. Hence, ω_{cam} is always equal to zero for linear camera motion. In the case of rotational camera motion, u_{cam} adds a rigid-body rotation to the real fluid motion. Hence, the vorticity ω_{cam} associated with rotational camera motion appears as a spatially uniform background vorticity (i.e., a constant vector) on top of which the real fluid vorticity is superimposed. By determining the level of background vorticity in regions away from the animal, this effect can be subtracted from the measurements. Notably, flow analyses based on Lagrangian coherent structures (LCS; e.g., Shadden et al. 2006; Peng et al. 2007) are inherently insensitive to both linear and angular camera motion because these constitute transformations of reference frame to which LCS are invariant by definition (Haller 2005).

To be sure, the effect of linear camera motion on the velocity field measurements can be corrected in an approximate fashion by first noting that in a volume V of fluid with rigid walls or in an unbounded flow (V → ∞) that is at rest at infinity,

$$\overline{u_{real}} = 0, \tag{2}$$

where the overbar denotes a spatial average over the volume V (Smits 2000). Taking the spatial average of Eq. 1 over the volume V and applying Eq. 2,

$$\overline{u_{scuva}} = \overline{u_{cam}} = u_{cam}, \tag{3}$$

since u_{cam} is spatially uniform for linear motions of the camera. Hence,

$$u_{real} \approx u_{scuva} - \overline{u_{scuva}}. \tag{4}$$

Equation 4 is presented as an approximation because strict equality only holds in the aforementioned cases of a bounded flow with rigid walls or in a flow at rest at infinity. By contrast, the SCUVA measurements capture only a small subset of the bounded flow (i.e., the landlocked marine environment), and although the flow may be at rest far from the animal, the total volume of fluid measured in the field of view is finite. The error associated with the correction is dependent on the animal size relative to the viewing window and on the spatial average of the velocity field that the animal creates. To see this, first note that the contributions from the velocity field of the animal (u_{real}) and the camera motion (u_{cam}) to the spatially averaged velocity field measured by SCUVA ($\overline{u_{scuva}}$) are given by

$$\overline{u_{scuva}} = \frac{1}{A_{win}} \int_{win} \left(u_{real} + u_{cam} \right) dA, \tag{5}$$

where A_{win} is the area of the measurement window and the effect of spatially uniform currents through the measurement window is included in u_{cam}. If we assume that the velocity field of the animal dominates a region of characteristic area A_{ani} in the measurement window, then Eq. 5 can be rewritten as

$$\overline{u_{scuva}} = \left(\frac{A_{win} - A_{ani}}{A_{win}} \right) \overline{u_{cam}} + \left(\frac{A_{ani}}{A_{win}} \right) \overline{u_{real}}, \tag{6}$$

where the overbars indicate spatial averages of the velocity fields. From this relationship, we see that the camera motion-correction given by Eq. 4 in the manuscript subtracts both the camera motion and a portion of the real velocity field created by the animal. This latter subtraction may be considered the error ε of the motion correction and can be expressed relative to the total error correction $\overline{u_{scuva}}$ as

$$\varepsilon = \left(\frac{A_{ani}}{A_{win}} \right) \left(\frac{\overline{u_{real}}}{\overline{u_{scuva}}} \right). \tag{7}$$

This error becomes small if $A_{ani} << A_{win}$ (i.e., the region of flow created by the animal is small relative to the measurement window size) and/or if the average velocity of the flow created by the animal is small (i.e., $\overline{u_{real}} << \overline{u_{scuva}}$). The latter condition may be difficult to evaluate a priori, but could be estimated based on existing models for the swimming of the target species. For example, since the momentum of the fluid set into motion by an animal starting from rest will be approximately equal and opposite to the momentum of the swimming animal itself, the magnitude of $\overline{u_{real}}$ can be estimated in this case as

$$\overline{u_{real}} \sim \frac{A_{body}}{A_{ani}} U_{body}, \tag{8}$$

where A_{body} is the area of the animal body in the field of view and U_{body} is the velocity that the animal achieves starting from rest.

Since the SCUVA measurements are based on two-dimensional DPIV, certain camera motions cannot be corrected by using Eq. 4 or any other method. Specifically, linear and/or angular motions of the camera that cause the flow to pass out of the plane of the laser sheet during a measurement cannot be compensated because the out-of-plane flow results in particle loss in the DPIV image cross-correlation. Due to this limitation of two-dimensional DPIV, measurements must be conducted in a manner that minimizes out-of-plane motions of particles in the camera field of view. In practice, the light sheet must be oriented such that the target animal swims parallel to it. The SCUBA diver must be especially careful not to move the device forward or backward during the measurement; panning of the camera while maintaining the laser sheet in the same plane is allowable if necessary. The laser sheet is a useful indicator of

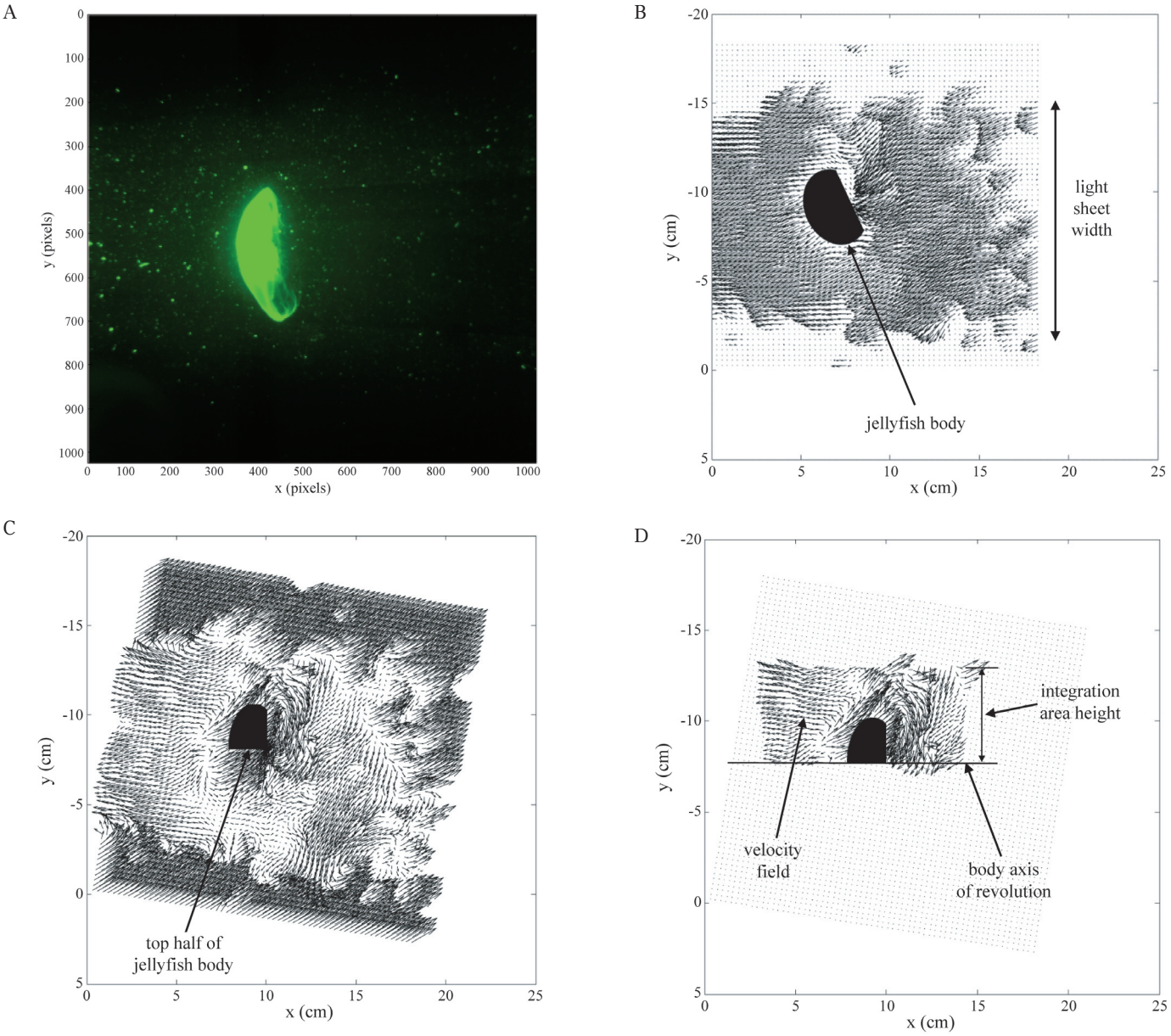

Fig. 3. (a) Raw image captured by SCUVA at time t = 0.633 s; (b) Corresponding velocity field at time t = 0.633 s. Position of animal in velocity field is indicated in overlay; (c) Rotated velocity field at time t = 0.633 s; (d) Corresponding rotated velocity field within an integration region equal to twice the bell radius.

out-of-plane motions since the location at which the laser sheet intersects the animal is clearly visible and will change in the event of out-of-plane motion. As with any measurement technique, the skill of the operator is refined with practice.

The body axis of a medusa swimming in the laser sheet is typically oriented at an angle θ with the horizontal. To simplify the subsequent data analyses, the instantaneous velocity fields were rotated by an angle $-\theta$ to align the animal's body axis with the horizontal. Assuming radial flow symmetry, data within a cylinder of radius R surrounding the animal were then used to compute spatial integrals of the velocity field. Figure 3 illustrates this post-processing as applied to the velocity field at time t = 0.633 s after the start of a swimming cycle (i.e., the initiation of bell contraction). Figure 3(a) shows the raw image captured via SCUVA. The corresponding velocity field is shown in Fig. 3(b). The effect of camera motion can be seen in the relatively large velocity vectors that appear upstream from the animal where the real flow was relatively quiescent. These vectors are absent at the top and bottom of the field of view due to the lack of laser illumination in those regions; the width of the laser sheet is indicated by the abrupt transition from large to small velocity vectors at the upper and lower margins of the measurement window. Fig. 3(c) shows the velocity field after the camera motion correction (i.e., Eq. 4) is implemented and the data are

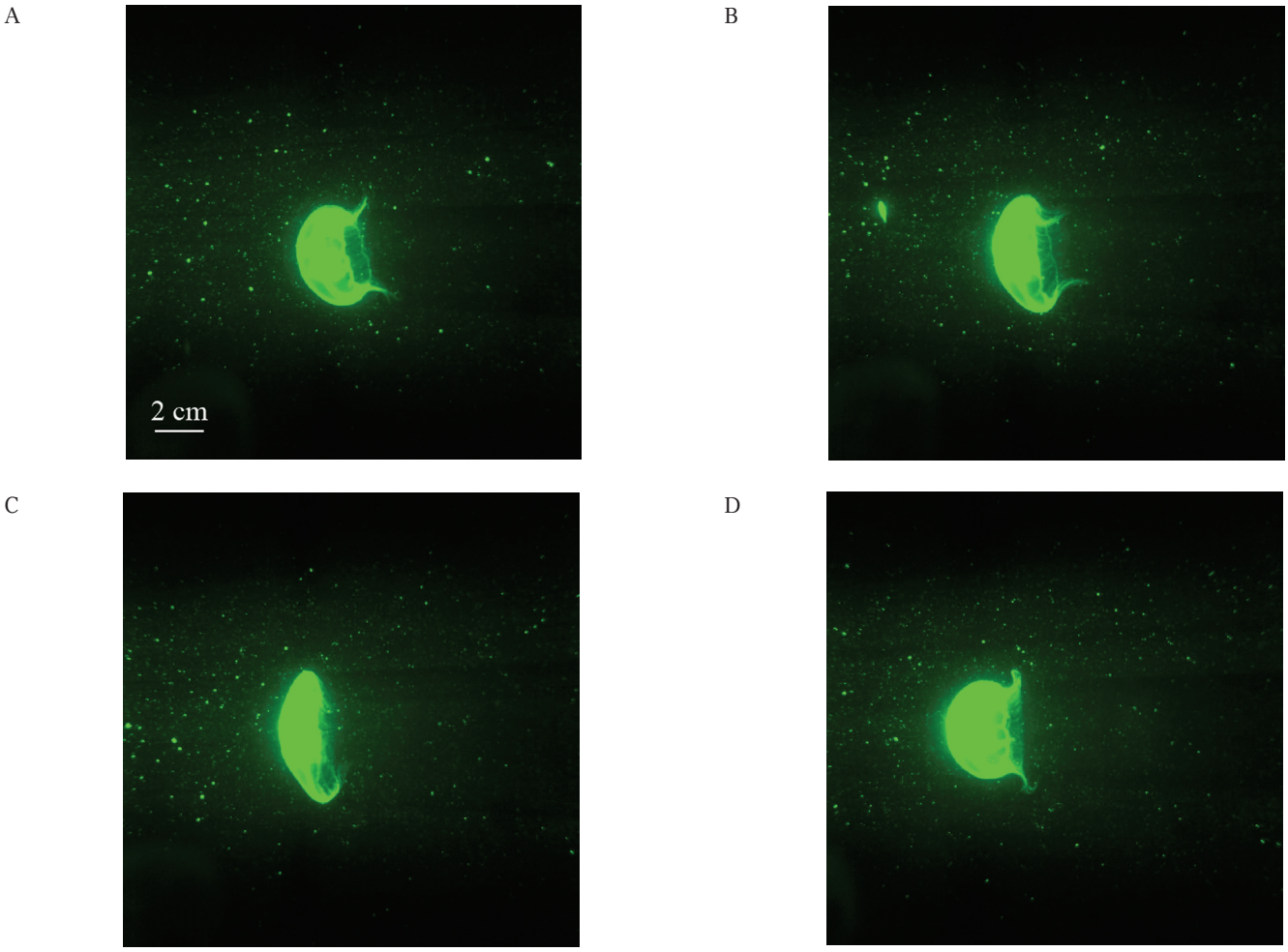

Fig. 4. Selected images of a single swimming cycle captured by SCUVA at time (from left to right, top to bottom): t = 0 s, t = 0.267 s, t = 0.533 s, and t = 0.967 s

rotated to orient the animal body axis horizontally. Finally, the integration area is identified in Fig. 3(d).

The velocity field in the selected cylindrical region of fluid around the animal was integrated to determine the instantaneous kinetic energy ($E_{ke}(t)$) in the flow:

$$E_{ke} = \frac{1}{2}\rho\int_V u_{real}^{\ 2}(t)\,dV \tag{9}$$

Since the animal is the only object in the region V and net advection through the region is observed to be small, it can be inferred that increases in the local kinetic energy are due to the swimming motions of the animal. Therefore, we can deduce the transient energetic effects of the animal-fluid interaction by using the SCUVA measurements.

Huntley and Zhou (2004) proposed a model to estimate the kinetic energy transferred to the fluid surrounding an aquatic animal during locomotion. In this model, the rate of kinetic energy transfer e_d is defined as

$$e_d = Du_c, \tag{10}$$

where D is the hydrodynamic drag on the animal and u_c is the cruising speed of the swimming animal. The total drag D caused by flow separation, surface friction, and loss of energy in the wake of the animal is defined in their model as

$$D = \frac{1}{2}\rho u_c^{\ 2} S_w C_D, \tag{11}$$

where ρ is the density of seawater (ρ = 1025 kg m^{-3}), S_w is the average total wetted surface area, and C_D is the drag coefficient. We note that Eq. 10 neglects the unsteady effects of animal propulsion and utilizes average values only. As will be shown below, this is a major limitation of their model (Daniel 1983). Their model also utilizes the empirical result that, for turbulent flow, the drag coefficient of a flat plate parallel to the flow is given by

$$C_D = 0.072\,Re^{-0.2}, \tag{12}$$

where Re is the Reynolds number. The Re is defined as $Re = \frac{u_c L}{\nu}$, where L is the characteristic length scale of the animal and ν is the kinematic viscosity of seawater ($\nu = 1.18 \times 10^{-6}$ m^2 s^{-1}).

Although the drag model of Huntley and Zhou (2004) is simplified, it enabled the authors to compare a broad range of aquatic species without concern for differences in morphology and kinematics. We use the same drag model here to provide a

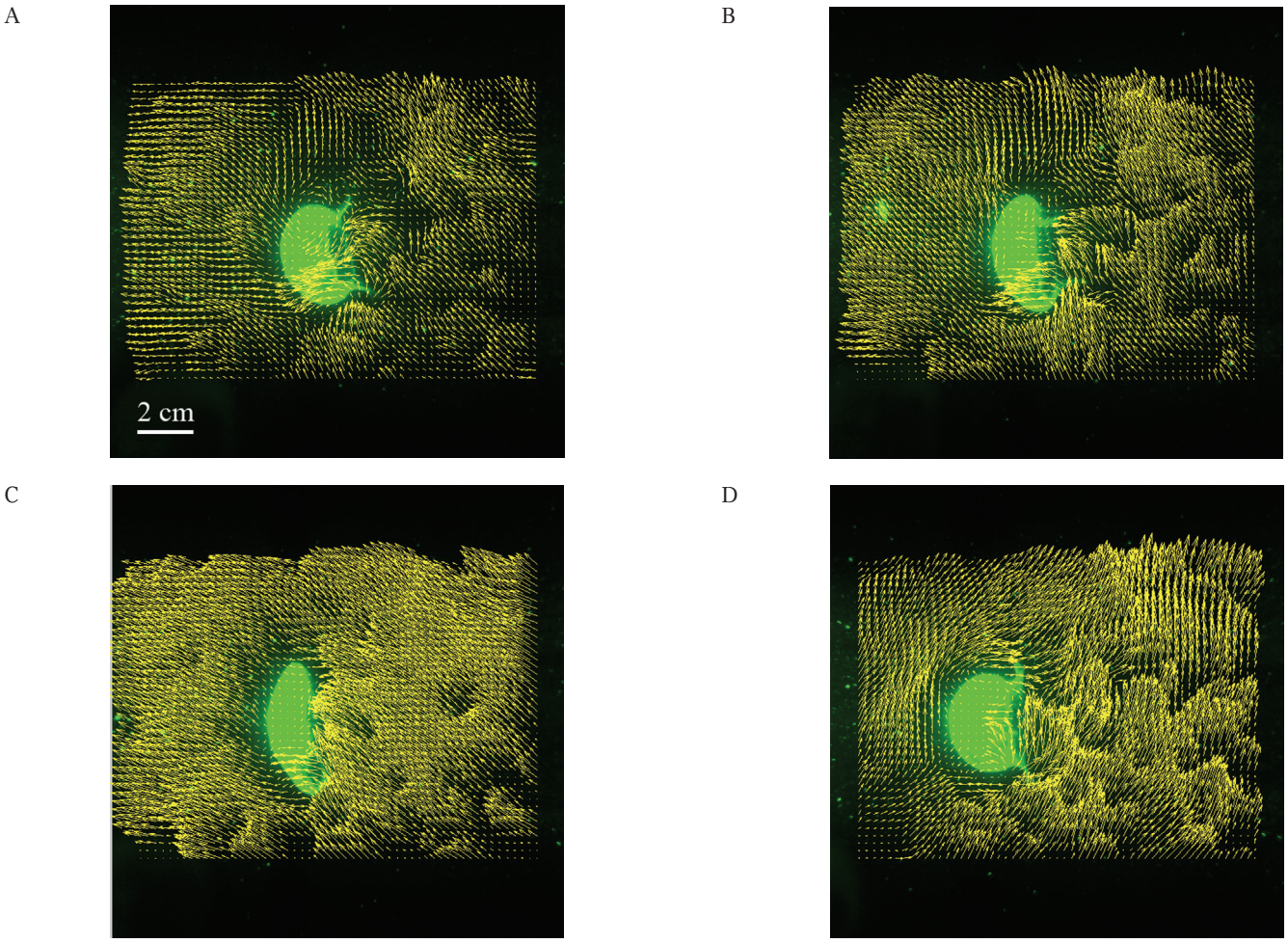

Fig. 5. Uncorrected velocity fields at time (from left to right, top to bottom): t = 0 s, t = 0.267 s, t = 0.533 s, and t = 0.967 s

comparison with the SCUVA measurements. We assume that the medusa body can be modeled as an axisymmetric, truncated ellipsoid. Therefore, the parameter S_w corresponds to the average surface area of an equivalent truncated ellipsoid and the characteristic length L is the average exit diameter of the animal. Using these parameters and the measured swimming speed of the animal, the model predicts a kinetic energy transfer given by the integral of energy transfer rate e_d integrated with respect to time t:

$$E_d = \int e_d dt = 0.036 \rho u_c^3 S_w \left(\frac{u_c L}{\nu} \right)^{-0.2} t . \qquad (13)$$

Figure 4 shows a series of images taken by SCUVA during a single swimming cycle. A color map matching the 532 nm laser output has been added to the images to show what is seen by SCUBA divers operating SCUVA during a night dive. The medusa in the view is swimming from right to left. The swimming cycle starts (t = 0 s) with the relaxation phase, where the bell exit begins to expand radially outward. At the end of the relaxation phase (t = 0.6 s), the animal's morphology reaches its most oblate form. At t = 0.633 s, the animal begins to contract its bell and continues to do so until the end of the swimming cycle. A series of images with the uncorrected and corrected velocity field can be found in figures 5 and 6, respectively. The measured velocity fields are qualitatively consistent with laboratory measurements of the same and similar species of *Aurelia* (Shadden et al. 2006; Franco et al. 2007). However, the significant background environmental flow features observed via SCUVA are necessarily absent from previous laboratory studies conducted in artificial flow environments.

The effect of the cylindrical integration region size on the fluid energy measurement can be seen in Fig. 7. The data points labeled "top" and "bottom" correspond to the selection of the integration area above and below the body axis, respectively. If the flow exhibits radial symmetry, integration of the top-or bottom-half of the flow field should yield the same result. For the integration height equal to the maximum bell radius over the swimming cycle R (top or bottom 1*R*), there is asymmetry between the top and bottom flow fields that may reflect asymmetry in the animal swimming kinematics. As the integration height is increased to 3*R*, we see that the flow becomes more symmetrical. This is expected since the contribution of the asymmetric animal motion to the total fluid energy decreases as the integration height increases.

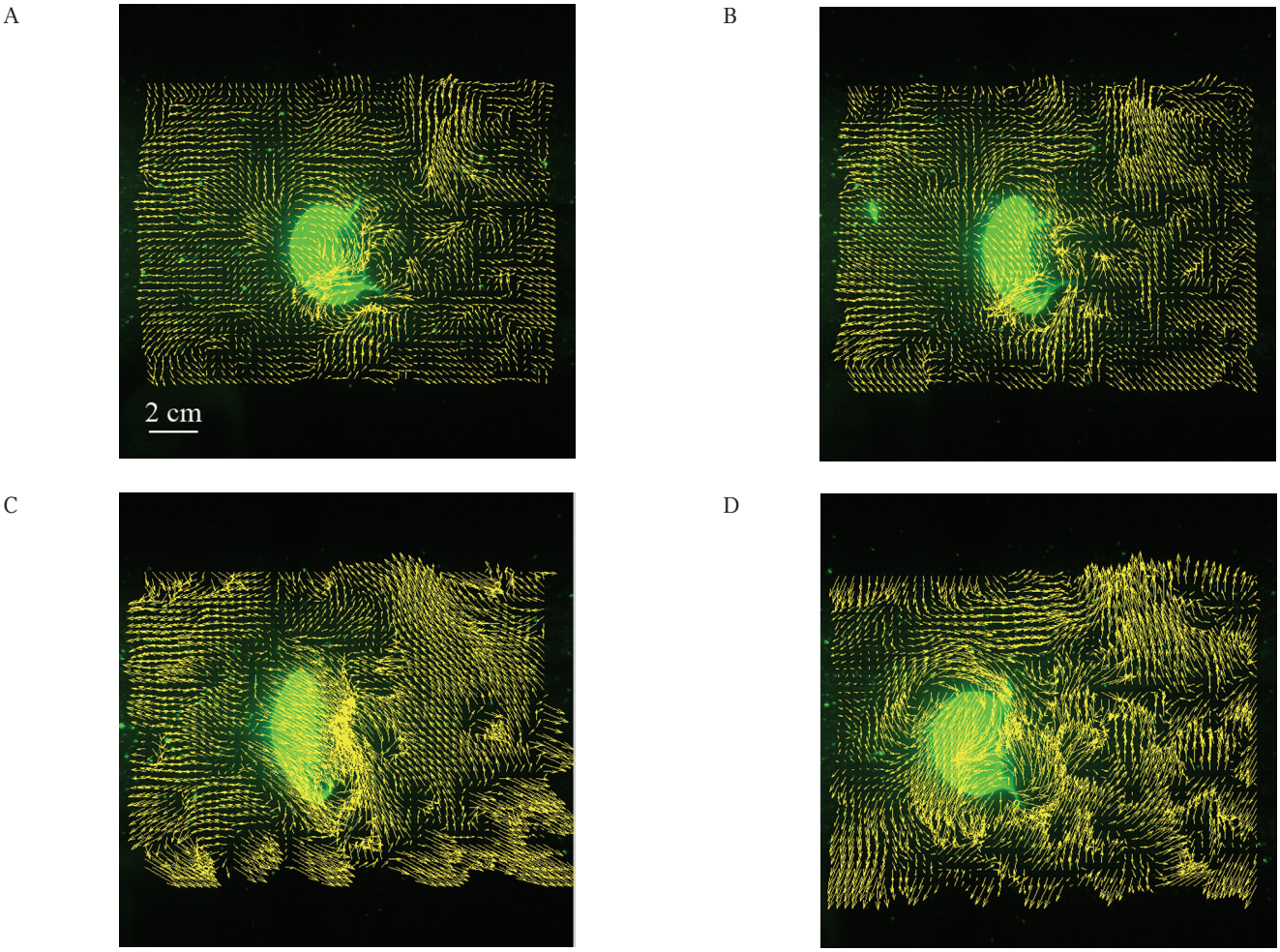

Fig. 6. Corrected velocity fields at time (from left to right, top to bottom): t = 0 s, t = 0.267 s, t = 0.533 s, and t = 0.967 s

In Fig. 8, we compare the SCUVA measurements for an integration height of 2R with the model proposed by Huntley and Zhou (2004). We find that direct SCUVA measurements of the energetics of animal-fluid interactions are consistent with the Huntley-Zhou model and that the model may in fact underestimate the transient energetics. The model approximates the animal body shape as a flat plate, which yields a conservative estimate of C_D, especially in light of its neglect of unsteady fluid dynamics. The simplistic drag model is likely a main source of the underestimated kinetic energy input during swimming. Additionally, the model assumes that S_w and Re (L and u_c) are constant in time (using the averaged value over the duration of swimming), when in fact the quantities vary during the swimming cycle of a jellyfish due to morphology shape changes and the inherent unsteadiness in periodic motion. Neglecting these effects precludes the possibility of a time-dependent energy prediction by the Huntley-Zhou model.

Unlike the Huntley-Zhou model that predicts a steady, linear increase in kinetic energy over time, SCUVA measurements reveal nonlinear variations in kinetic energy of the fluid over a swimming cycle. In the absence of energy dissipation, the kinetic energy measurements should be monotonically increasing with time, irrespective of linearity. However, we observe a drop in the kinetic energy toward the end of the measurements. We hypothesize that these dynamics are the result of kinetic energy dissipation in the flow that occurs between swimming cycles. The temporal trend of kinetic energy dissipation can be expected to follow an exponential decay in time, with characteristic time scale L/u_c (Tennekes and Lumley 1972):

$$E_{ke}(t) = E_0 \exp\left[-Bt\left(\frac{u_c}{L}\right)\right], \tag{14}$$

where E_0 is the initial kinetic energy and B is a constant of order one. Comparison of the SCUVA measurements with this predicted temporal behavior supports the conclusion that kinetic energy dissipation is prominent in this flow (Fig. 8). This result is relevant to the ocean-mixing problem because kinetic energy that is dissipated on fast time scales can only contribute to mixing in regions in very close proximity to the animal responsible for the energy input. In contrast, kinetic energy that persists over longer time scales has the potential

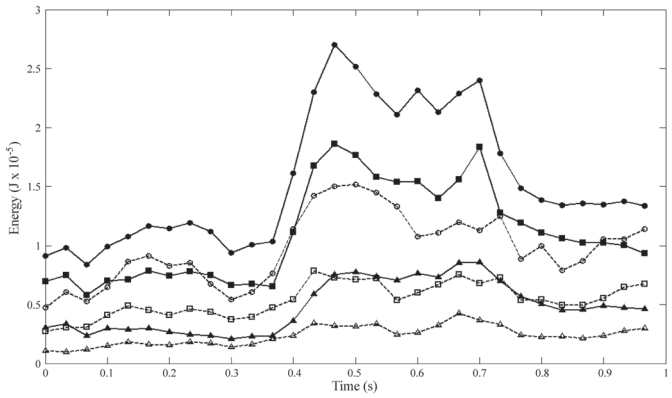

Fig. 7. Effect of the integration volume on the calculated kinetic energy in the fluid. Solid lines and filled symbols, integration of velocity field above the animal; dashed lines and open symbols, integration of velocity field below the animal. The radius of the integration is increased by integer multiples of the jellyfish radius (*R*): triangles, 1*R*; squares, 2*R*; circles, 3*R*.

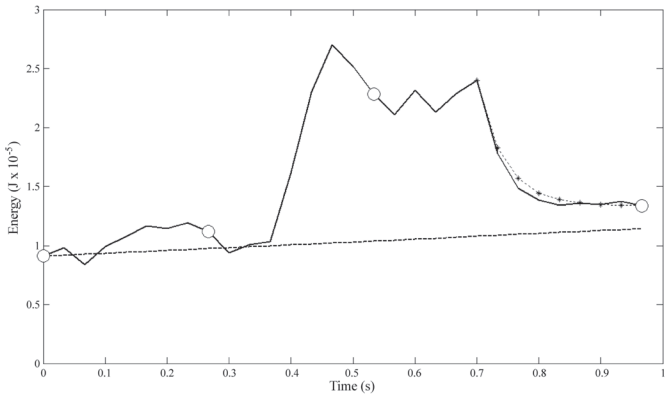

Fig. 8. Comparison of model (i.e., Huntley and Zhou [2004]) and measurement of fluid kinetic energy induced by animal swimming over a single swimming cycle. Dashed line, Huntley-Zhou model; solid line, SCUVA measurement; dotted line with filled circles, predicted kinetic energy dissipation (see text, cf Tennekes and Lumley [1972]). Open circles indicate energy values at times corresponding to t = 0 s, t = 0.267 s, t = 0.533 s, and t = 0.967 s.

to be advected from the site of its input to the ocean and therefore to affect mixing in regions that are removed geographically from the animals. Inspection of the characteristic time scale suggest that this type of "remote biogenic mixing" can be achieved by animals that are large and/or slow moving. These hypotheses will require the support of additional empirical data before they can be accepted conclusively. SCUVA provides a means to achieve the necessary data.

Discussion

We have demonstrated the potential utility of SCUVA as a quantitative, laboratory-quality device to analyze animal-fluid interactions in the field. Although the present proof-of-concept focused specifically on energetic issues, the technique has the potential to provide much needed empirical data in cases where laboratory data cannot be obtained (e.g., due to animal fragility) and in cases where laboratory studies are insufficient to quantify animal-fluid interactions as they occur in situ. Examples of such studies include, but are not limited to, interspecific differences in foraging behavior, predator-prey encounters in a realistic turbulent media, energetics of locomotion, etc.

A unique challenge in the development of this technique is the lack of existing field data for many of the processes to be investigated using SCUVA. As such, validation of the SCUVA measurements necessarily relies on qualitative comparisons with laboratory measurements of similar processes. In the present case, we find that the velocity field immediately surrounding the swimming animal is similar to the velocity field measured in previous laboratory studies (Shadden et al. 2006; Franco et al. 2007). However, the turbulent background flow is unique to the field measurements, since these environmental features are absent from the controlled laboratory flows. This background flow is a significant feature of animal-fluid interactions in real marine environments, and SCUVA provides a means to quantify these local, transient features in real time.

Comments and recommendations

The primary limitation of the current SCUVA device is its inability to measure full three-dimensional flow fields. This challenge is general to the field of fluid flow measurement as a whole. Work is underway to apply recently developed defocusing DPIV techniques (Pereira et al. 2006) in order to enable three-dimensional measurements using SCUVA. Another potential obstacle to widespread use of this version of SCUVA is its cost. The apparatus described herein costs approximately 90K USD, primarily due to the specialized portable camera that is used. However, in collaboration with J. H. Costello (Providence College) and S. P. Colin (Roger Williams University), we have recently field-tested a miniature, second generation version of SCUVA whose cost is reduced by more than an order of magnitude, to approximately 7K USD. This device uses an off-the-shelf camcorder (Sony HDR-HC7) within an underwater housing (Amphibico Dive Buddy EVO HD Elite) as the flow imager. This miniature SCUVA has a lower frame rate (60 fps standard, or 240 fps for up to 3 s), which may limit its ability to capture very fast fluid motions. Nonetheless, in our recent studies of fast-jetting medusan jellyfish that can swim up to 10 body lengths per second, we have not encountered cases in which camera speeds greater than 60 fps were necessary to resolve the flow. Additional benefits of the miniature SCUVA system are that it records to digital video (DV) tape, enabling continuous recording for up to 1 h; it includes a built-in video display such that the operator can ensure the target organism is in the camera's field of view; and its size, weighing only 5 kg out of the water. A long-term study is underway using this second generation device, the results of which will be described in a future publication.

References

Adrian, R. J. (1991) Particle-imaging techniques for experimental fluid-mechanics. Ann. Rev. Fluid Mech. 23:261-304.

Agrawal, Y. C., and H. C. Pottsmith. (1994) Laser diffraction particle sizing in STRESS. Cont. Shelf Res. 14(10/11): 1101-1121.

Bartol, I. K., M. R. Patterson, and R. Mann. (2001) Swimming mechanics and behavior of the shallow-water brief squid Lolliguncula brevis. J. Exp. Biol. 204:3655-3682.

Bertuccioli, L., G. I. Roth, J. Katz, and T. R. Osborn. (1999) A submersible particle image velocimetry system for turbulence measurements in the bottom boundary layer. J. Atmos. Ocean. Tech. 16:1635-1646.

Bundy, M. H., and G. A. Paffenhofer. (1996) Analysis of flow fields associated with freely swimming calanoid copepods. Mar. Ecol. Prog. Ser. 133:99–113.

Catton, K. B., D. R. Webster, J. Brown, and J. Yen. (2007) Quantitative analysis of tethered and free-swimming copepodid flow fields. J. Exp. Biol. 210:299-310.

Clarke, J., A. Cotel, and H. Tritico. (2007) Development, testing and demonstration of a portable submersible miniature particle imaging velocimetry device. Meas. Sci. Technol. 18:2555-2562.

Dabiri, J. O., S. P. Colin, J. H. Costello, and M. Gharib. (2005) Flow patterns generated by oblate medusan jellyfish: field measurements and laboratory analyses. J. Exp. Biol. 208(7): 1257-1265.

——— and M. Gharib. (2004) Fluid entrainment by isolated vortex rings. J. Fluid Mech. 511:311-331.

Daniel, T. L. (1983) Mechanics and energetics of medusan jet propulsion. Can. J. Zool. 61:1406-1420.

Dewar, W. K., R. J. Bingham, R. L. Iverson, D. P. Nowacek, L. C. St. Laurent, and P. H. Wiebe. (2006) Does the marine biosphere mix the ocean? J. Mar. Res. 64:541-561.

Didden, N. (1979) On the formation of vortex rings: Rolling-up and production of circulation. J. App. Math. Phys. 30:101-116.

Drucker, E. G., and G. V. Lauder. (1999) Locomotor forces on a swimming fish: three-dimensional vortex wake dynamics quantified using digital particle image velocimetry. J. Exp. Biol. 202:2393-2412.

Emlet, R. B. (1990) Flow fields around ciliated larvae: effects of natural and artificial tethers. Mar. Ecol. Prog. Ser. 63:211-225.

Franco, E., D. N. Pekarek, J. Peng, and J. O. Dabiri. (2007) Geometry of unsteady fluid transport during fluid-structure interactions. J. Fluid Mech. 589:125-145.

Haller, G. (2005) An objective definition of a vortex. J. Fluid Mech. 525:1-26.

Huntley, M. E., and M. Zhou. (2004) Influence of animals on turbulence in the sea. Mar. Ecol. Prog. Ser. 273:65-79.

Katija, K., and J. O. Dabiri. (2006) Dynamics of tethered versus free-swimming animals: A wake structure comparison in jellyfish. Proc. Amer. Phys. Soc. Div. Fluid Dyn. Bull. Amer. Phys. Soc. 52(12):59.

Katz, J., P. L Donaghay, J. Zhang, S. King, and K. Russell. (1999) Submersible holocamera for detection of particle characteristics and motions in the ocean. Deep-Sea Res. 46:1455-1481.

Koehl, M. A. R., and J. R. Strickler. (1981) Copepod feeding currents: food capture at low Reynolds number. Limnol. Ocean. 26(6):1062-1073.

Kunze, E., J. F. Dower, I. Beveridge, R. Dewey, and K. P. Bartlett. (2006) Observations of biologically generated turbulence in a coastal inlet. Science 313:1768-1770.

Munk, W., and C. Wunsch. (1998) Abyssal recipes II: energetics of tidal and wind mixing. Deep-Sea Res. 45:1977-2010.

Munk, W. H. (1966) Abyssal recipes. Deep-Sea Res. 13:707-730.

Nimmo Smith, W. A. M., P. Atsavapranee, J. Katz, and T. R. Osborn. (2002) Piv measurements in the bottom boundary layer of the coastal ocean. Exp. Fluids 33:962-971.

Peng, J., Dabiri, J. O., Madden, P. G. and Lauder, G. V. (2007) Non-invasive measurement of instantaneous forces during aquatic locomotion: a case study of the bluegill sunfish pectoral fin. J. Exp. Biol. 210:685-698.

Pereira, F., H. Stuer, E. C. Graff, and M. Gharib. (2006) Two-frame 3d particle tracking. Meas. Sci. Technol. 17:1680-1692.

Shadden, S. C., J. O. Dabiri, and J. E. Marsden. (2006) Lagrangian analysis of fluid transport in empirical vortex rings. Phys. Fluids 18(4):047105-1-047105-11.

Smits, A. J. (2000) A physical introduction to fluid mechanics. New York: John Wiley and Sons.

Steinbuck, J. V., C. D. Troy, P. J. Franks, E. Karakoylu, J. S. Jaffe, S. G. Monismith, and A. R. Horner. (2004) Small-scale turbulence measurements with a free-falling DPIV profiler. Proc. Amer. Geophys. Union. Fall Meeting 2004, abstract #OS53B-05.

Tennekes, H., and J. L. Lumley. (1972) A first course in turbulence. Cambridge: MIT Press.

Tytell, E. D., and G. V. Lauder. (2004) The hydrodynamics of eel swimming. J. Exp. Biol. 207:1825-1841.

Vogel, S. (1966) Flight in *Drosophila*: I. flight performance of tethered flies. J. Exp. Biol. 44:567-578.

Willert, C. E., and M. Gharib. (1991) Digital particle image velocimetry. Exp. Fluids 10(4):181-193.

Yen, J., J. Brown, and D. R. Webster. (2003) Analysis of the flow field of the krill, *Euphausia Pacifica*. Mar. Fresh. Behav. Physiol. 36(4):307-319.

Submitted 12 July 2007
Revised 15 October 2007
Accepted 13 November 2007